PHYSICS AND CHEMISTRY OF SOLID STATE
V. 27, No.1 (2026) pp. 108-117
Section: Chemistry

DOI: 10.15330/pcss.27.1.108-117

Vasyl Stefanyk Carpathian National University

ФІЗИКА І ХІМІЯ ТВЕРДОГО ТІЛА
Т. 27, № 1 (2026) С. 108-117
Хімічні науки

PACS: 81.05.Mh

ISSN 1729-4428 (Print)
ISSN 2309-8589 (Online)

O.M. Yanchuk[1], O.V Smitiukh[2], O.V. Marchuk[2], S.V. Suprunovich[2], V.M. Kordan[3]

The Effect of Thiourea Concentration on Chemical Composition, Morphology and Nanocomposite Particle Distribution ZnO/ZnS Obtained by Electrochemical Anodizing Method

[1]*Volyn Medical Institute, Lutsk, Ukraine, yanchuk59@gmail.com*
[2]*Lesya Ukrainka Volyn National University, Lutsk, Ukraine, Smitiukh.Oleksandr@vnu.edu.ua*
[3]*Ivan Franko National University of Lviv, Lviv, Ukraine, vasyl.kordan@lnu.edu.ua*

The presented study systematically investigated the influence of different thiourea (TU) concentrations on the synthesis and properties of ZnO/ZnS nanocomposites using an electrochemical anodization method. TU acted as a source of sulfur, allowing ZnS to form within the ZnO matrix. Structural, morphological, and compositional analyses were carried out using techniques such as X-ray diffraction (XRD), a Tescan Vega3 LMU microscope, ImageJ software with ParticleSizer (for large crystals) and MorphoLibJ (for background) plug-ins, and energy dispersive X-ray spectroscopy (EDX). Chemical composition analysis confirmed that the increase of the concentration of TU leads to an increase in the content of ZnS. Elevating the concentration of TU in the electrolyte alters the makeup of the composite powders, shifting the balance from a predominance of lighter particles to a greater proportion of background particles within the mixture. This adjustment also leads to a significant reduction in the dimensions of the lighter particles, decreasing their length by half and their width by 1.5 times. Furthermore, this change in particle composition and size can have implications for the overall properties and performance of the composite materials. The parameters μ and σ decreases with the increase of the concentration of TU, and it testify that particles are, on average, getting smaller and more uniform in size. The mode and median values follow this trend, decreasing consistently across the series, confirming the presence of finer and more monodisperse particles in samples 6–8. Understanding these relationships is crucial for optimizing material formulations to meet specific requirements in fields such as electronics, energy storage, and advanced manufacturing.

Keywords: thiourea, nanocomposites, anodizing, morphology.

Received 14 May 2025; Accepted 05 February 2026; Published 10 March 2026.

Introduction

The synthesis of nanocomposites based on zinc oxide (ZnO) and zinc sulfide (ZnS) has attracted significant attention in modern science due to their unique electronic, optical, and catalytic properties. [1-3].

The application of such materials is becoming increasingly widespread; especially it is used for the solar system and the sensor technology [4-5]. The application of the electrochemical anodising method has been identified as a prospective approach for the fabrication of nanocomposites of ZnO/ZnS [6]. This method enables the modulation of both the morphology and chemical composition of the resultant materials through the precise manipulation of the reaction conditions.

It is imperative to acknowledge the pivotal role of the TU concentration on the characteristics of the synthesized nanocomposites. TU functions as a stabiliser and a source of sulfur during the synthesis process, thereby exerting a significant influence on the properties of the nanocomposites. Research findings indicate that alterations in the substance's concentration can result in substantial changes to the morphological characteristics, particle distribution, and chemical composition of the resulting materials. For instance, as demonstrated in the work of Chen et al. (2021), optimisation of TU

concentration has been shown to enhance the electrical properties of nanocomposites, thereby unveiling novel prospects for their application in electronic applications [7].

This work constitutes a logical continuation of the study [6], in which the results of X-ray phase analysis of a mixture of ZnO and ZnS particles and the thickness of these particles, calculated using the Scherrer method [8], were published. The paper mentioned above [6] describes the electrochemical synthesis of a 1M aqueous solution of sodium chloride with varying TU content. This synthesis is carried out by electrolysis, with a soluble zinc anode and constant current density, temperature, and process duration. X-ray diffraction analysis was employed to ascertain the nature of the products of zinc anodization. This analysis revealed that the products are nanosized zinc oxide and zinc sulfide particles. It has been demonstrated that an increase in TU concentration decreases the thickness of the formed particles. The product is primarily powdery zinc oxide at the lowest concentrations of TU in the electrolyte, while at the highest concentrations, it is predominantly zinc sulfide. The increase in TU in the sample facilitates the transformation of β-ZnO into α-ZnO, substituting oxygen atoms by sulfur atoms. The ZnS particles (1.3-3.6 nm) are significantly thinner than the ZnO particles (7-29 nm) [6].

The report of the results is about of energy dispersive X-ray microanalysis of the quantitative composition of zinc oxide and zinc sulfide in molar percent in each of the eight samples investigated. Furthermore, the analysis of photographs taken with a Tescan Vega3 LMU microscope [http://matersciimc.lnu.edu.ua/equipment/tescan/] for the same eight samples regarding the morphology and size of zinc oxide and zinc sulfide particles is provided. The photographic material was analysed using ImageJ software with the ParticleSizer (for large crystals) and MorphoLibJ (for background) plugins [9].

The object of the study is to examine the impact of TU concentration on the chemical composition, morphology, and nanocomposite particle distribution of ZnO/ZnS, which were synthesised by the electrochemical anodising method. The results of the investigation may serve as a foundation for future research.

I. Experimental details

The synthesis methodology of the obtained powder samples is described in detail in [6]. The samples of 8 powdered precipitates differed in the concentration of TU added to the electrolyte (Table 1).

The Tescan Vega3 LMU microscope (Czech Republic, Brno) is equipped with two detectors: SE and BSE. The surface scanning of the samples is performed using an electron beam (generated by a W thermionic cathode) with a diameter of a few nanometers and an acceleration voltage of 15-25 kV. The working distance from the gun to the sample in SEM mode is contingent on the required magnification, which for powders is between 10-15 mm. In SE detector mode (secondary electrons), the surface state (topographic contrast) of the sample can be assessed, while in BSE detector mode (backscattered secondary electrons), phases can be identified based on contrast according to the average atomic number. Phases with a higher number of electrons will appear brighter than phases based on elements with a lower atomic number. Prior to scanning, the powders were applied in a thin layer onto a conductive graphite film and purged with an inert gas. The study was conducted in conditions of isolation, i.e. in a vacuum (residual pressure < $9 \cdot 10^{-3}$ Pa).

The energy-dispersive X-ray microanalyzer is equipped with a drift Si semiconductor detector X-Max^{N}20 cooled by Peltier elements (Oxford Instruments Aztec ONE). It allows for quantitative determination of the integral composition of the sample and the distribution of elements across the surface, as well as the composition of each phase. The range of elements that can be detected by this method spans from Be to Cf at an operating voltage of 25-30 kV.

The R-statistics programme [9] was used to analyze the data obtained.

II. Discussion

Fig. 1 shows the results of energy dispersive X-ray analysis for sample 1 as an example.

As there may be an excess of oxygen due to the burning of the graphitised film, we focused on the content of zinc in determining the elemental content as it forms both oxide and sulphide according to X-ray diffraction data [6]. 30.55 atomic percent zinc is 4.30 percent sulphur, so there should be 30.55-4.30 = 26.25 atomic % oxygen. This gives a total of 61.1%. Next we convert this amount to 100%. So for all samples the zinc will be 50%. For sample 1 (0.5M TU) the sulphur content will be 4.30/61.1*100 = 7.0% and the oxygen content 26.25/61.1*100 = 43.0%.

As demonstrated by the EDS results, an increase in the concentration of TU from 0.5M to 4.0 M in the synthesized samples results in a decrease in the proportion of zinc oxide and an increase in the proportion of zinc sulfide (Table 2). A quantitative jump is observed for samples 7 and 8 (3.5 and 4.0 M TU, respectively). It is in these samples that there is more zinc sulfide than zinc oxide.

When synthesizing ZnO/ZnS nanocomposites via methods such as electrochemical anodizing, zinc oxide (ZnO) is often present initially, and the sulfur component (needed to form ZnS) is introduced via a sulfur-containing

Table 1.

Conditions for electrochemical synthesis of zinc anodization with varying TU content in the electrolyte. Constant synthesis conditions: temperature 90 °C; electrolysis time 20 minutes; current density 0.408 A/cm²; zinc anode, carbon cathode with a constant surface area of 5 cm²; 1M NaCl solution as the electrolyte

Number of experiment	1	2	3	4	5	6	7	8
[TU], M	0.5	1.0	1.5	2.0	2.5	3.0	3.5	4.0

compound—thiourea in this case.

Thiourea slowly decomposes in aqueous solutions under heating or electrochemical conditions to release sulfur species:

$$SC(NH_2)_2+H_2O \rightarrow H_2S+\text{other products}$$

$$Zn^{2+}+H_2S \rightarrow ZnS\downarrow+2H^+$$

These sulfur species readily react with Zn^{2+} ions or convert existing ZnO at the surface into ZnS via a replacement reaction:

$$ZnO_{(s)} + H_2S_{(aq)} \rightarrow ZnS_{(s)} + H_2O$$

This finding is consistent with the results of X-ray diffraction [6], which demonstrated that the synthesised samples are composed of ZnO/ZnS composites.

The photographs obtained by the SEM method are displayed in Figures 2 and 3.

The presented images demonstrate a downward trend in particle size with increasing TU concentration in the electrolyte during electrochemical synthesis. Specifically, there is a tendency to reduce the number of large particles while increasing the number of small particles. It is evident that the larger particles have a spindle-like shape. Furthermore, the presence of minute, round particles in close proximity to larger particles has been observed. In a previous study, for the samples analyzed in this work, it was found that the thickness of zinc oxide particles decreased from 29 to 7 nm, and zinc sulfide particles decreased from 3.6 to 1.2 nm with an increase in TU concentration from 0.5 to 3.0 M [6]. The trend of decreasing particle sizes is observed in the same range of TU concentration changes during the syntheses; however, it is visually problematic to distinguish between zinc oxide and zinc sulfide particles in this case.

The current work proposes an attempt to assess the distribution of the synthesised particles by width and length, and to separate the zinc oxide and zinc sulfide particles.

Preliminary analysis of the image yielded data in CSV format, encompassing descriptions of the detected

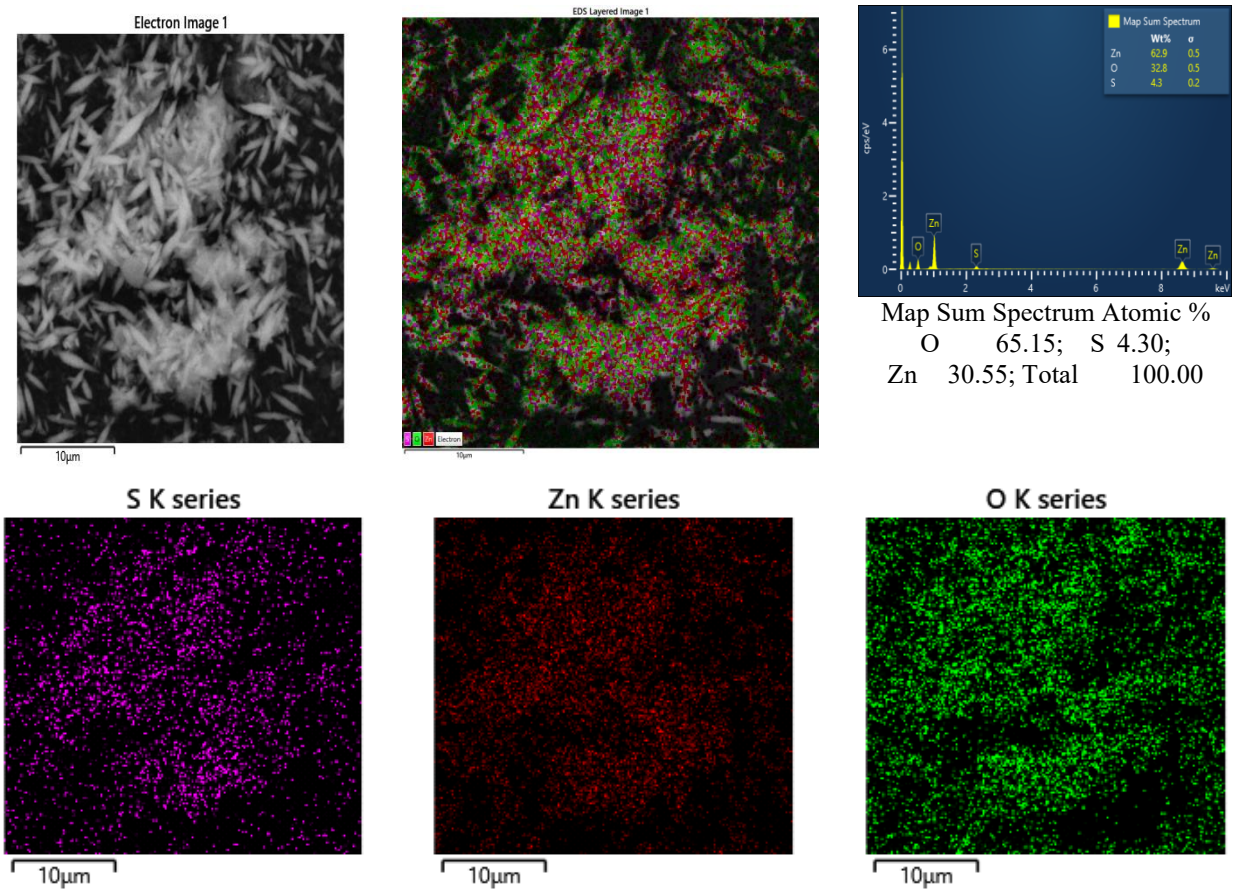

Fig. 1. Results of EDS analysis of sample 1 obtained by electrochemical anodizing method.

Table 2.

EDS results for determination of molar fractions of zinc, oxygen and sulfur, zinc oxide and zinc sulfide

№ of sample	1	2	3	4	5	6	7	8
[TU], M	0.5	1.0	1.5	2.0	2.5	3.0	3.5	4.0
χ_{Zn} (mol. %)	50.0	50.0	50.0	50.0	50.0	50.0	50.0	50.0
χ_{O} (mol. %)	43.0	37.8	32.5	32.4	31.0	30.1	14.6	12.1
χ_{S} (mol. %)	7.0	12.2	17.5	17.6	19.0	19.9	35.4	37.9
χ_{ZnO} (mol. %)	86.0	75.6	65.0	64.8	62.0	60.2	29.2	24.2
χ_{ZnS} (mol. %)	14.0	24.4	35.0	35.2	38.0	39.8	70.8	75.8

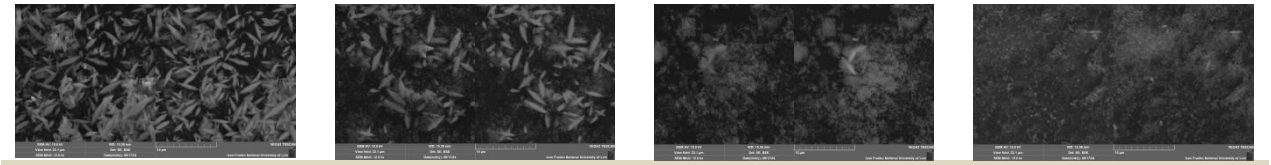

Fig. 2. SEM images of samples obtained at different concentrations of TU in the electrolyte, M: Sample 1 – 0.5; 2 – 1.0; 7 – 3.5; 8 – 4.0.

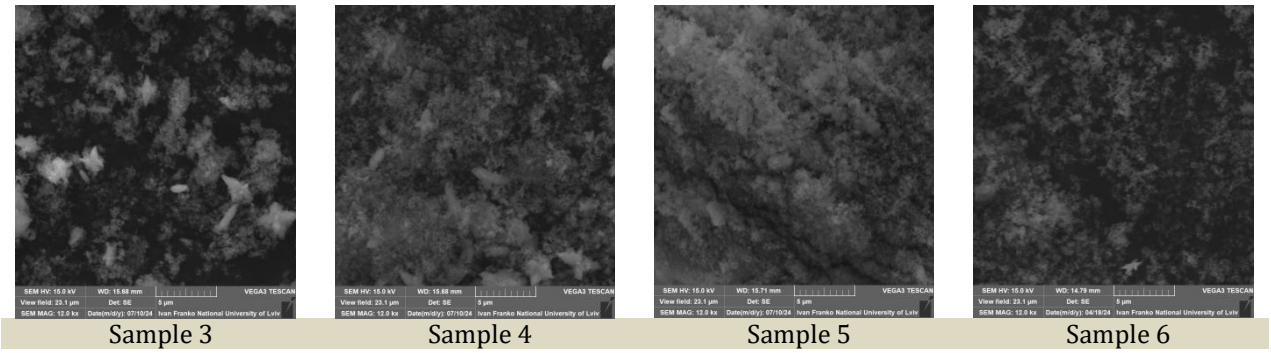

Fig. 3. SEM images of samples obtained at different concentrations of TU in the electrolyte, M: Sample 3 – 1.5; 4 – 2.0; 7 – 2.5; 8 – 3.0.

particles according to the following parameters: the following list comprises the labels, areas, means, standard deviations, modes, minima, maxima, x- and y-coordinates, x- and y-margins, perimeters, x- and y-axes, widths, heights, major and minor axes, angles, circularities, Feret lengths, integrated densities, medians, skewness, kurtosis, percentages of area, raw integrated densities, slices, Feret x- and y-axes, Feret angles, minima of Feret, arithmetic means, rounding, and solidity. The analysis was conducted using R-statistics software [9].

The MinFeret parameter was selected for the assessment of particle distribution due to its minimal reliance on particle orientation, thereby providing the most accurate representation of the distribution.

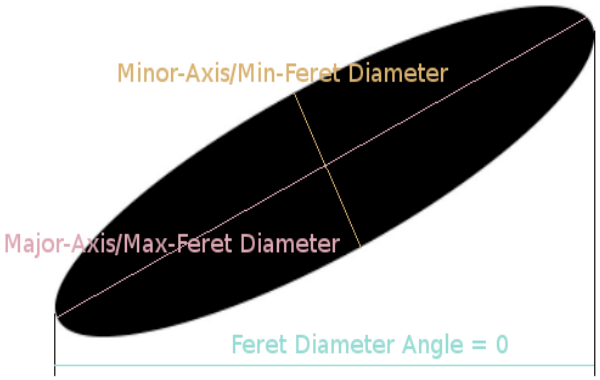

Fig. 4. Image of the width (MinFeret) and length of the particle (MaxFeret, hereafter Feret).

As demonstrated by the photographs, the left and right images were recognised separately in each picture (where they are present). The recognition data for the left and right images were combined and subsequently utilised for analysis.

For each sample, two histograms were constructed: the first characterises large bright crystals (suffix P), while the second represents weakly expressed structural elements of the background (suffix S). The histograms illustrate the distribution of particle sizes concerning the values of the MinFeret or Feret parameters.

The size data can be approximated by a log-normal distribution curve, with the parameters of this distribution being determined. The curve is plotted on the histogram. The parameters of this distribution are not physical; however, they can yield values that are physical and which characterize the size of the particles. These include the mode, which indicates the most typical particle size; the standard deviation, which characterises the width of the distribution; and the errors in determining the distribution parameters.

All sizes are presented in μm. To characterise the shape of the particles, graphs of relative particle length (the ratio of Feret/MinFeret, sorted in descending order) were constructed.

As demonstrated by the presented histograms and graphs, it is evident that light particles predominantly exhibit an elongated morphology, characterized by a length that is at least two times greater than the width.

Figure 13 presents an intriguing distribution of the light particles and the background particles.

As demonstrated by the presented histograms and graphs, it is evident that the background particles predominantly exhibit a rounded morphology, characterized by dimensions that do not exceed a disparity of 1.5 times the length and width measurements. As illustrated in Figure 13, a clear distinction is evident in the size of the background particles when compared to the light particles.

Both red and blue datasets show a clear positive correlation – as MinFeret increases, Feret also increases. The blue group is more tightly clustered along the diagonal (indicating more uniform or symmetric shapes).The red group shows a broader spread, especially in Feret values – suggesting greater variability in particle elongation or shape. A few red dots have high Feret values even at lower MinFeret – possible elongated or irregular particles.

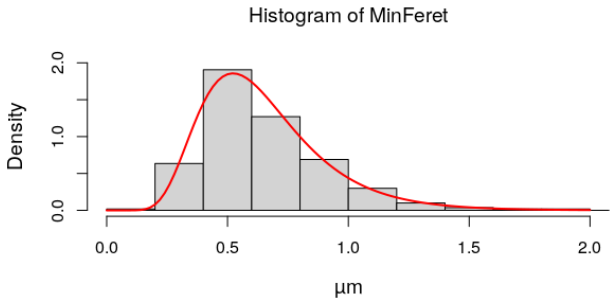

Fig.5. Histogram of the light crystals by width.

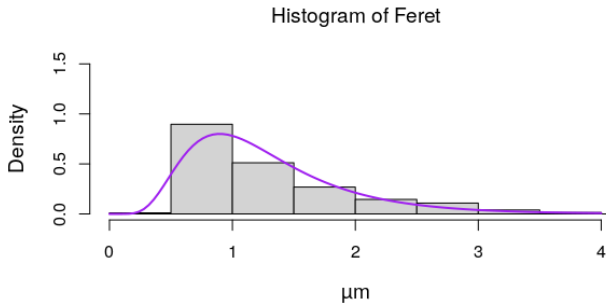

Fig.6. Histogram of the light crystals by length.

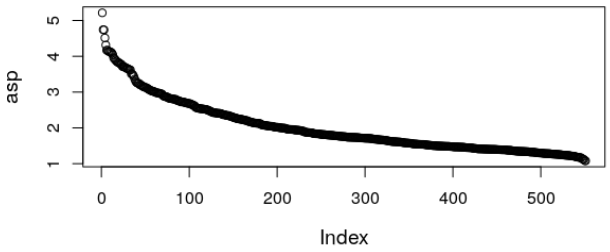

Fig.7. Distribution graph of the ratio of particle length to width with increasing number of the light particles.

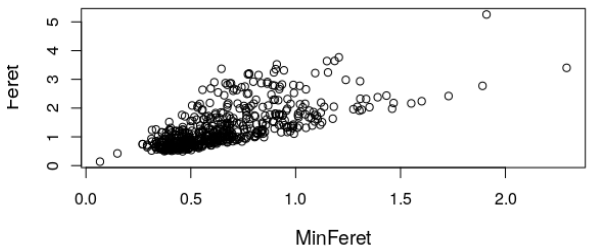

Fig.8. Distribution of the number of the light particles according to their size.

Figs. 5-8. Characterization of the light particles in sample 1.

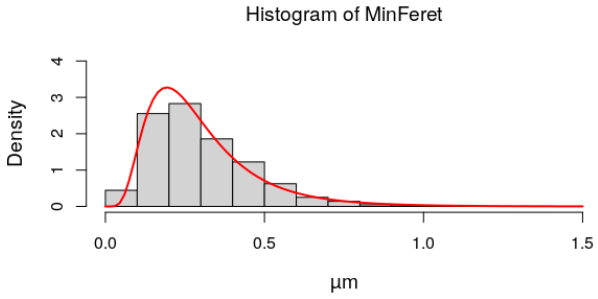

Fig.9. Histogram of background crystals by width.

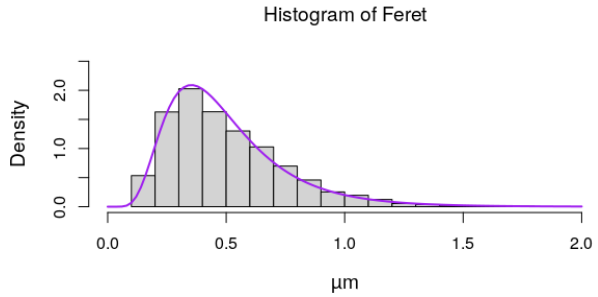

Fig.10. Histogram of background crystals by length.

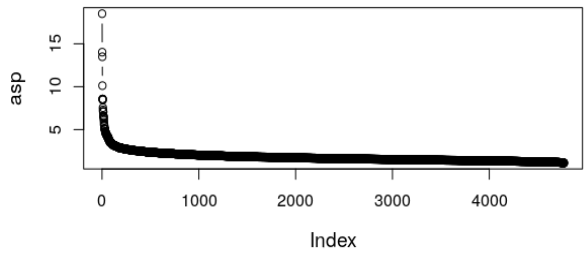

Fig.11. Distribution graph of the ratio of particle length to width with increasing number of the background particles.

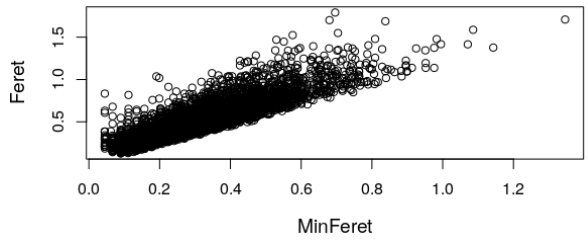

Fig.12. Size distribution of the background particles by the sizes.

Fig. 9-12. Characterization of the background particles in sample 1.

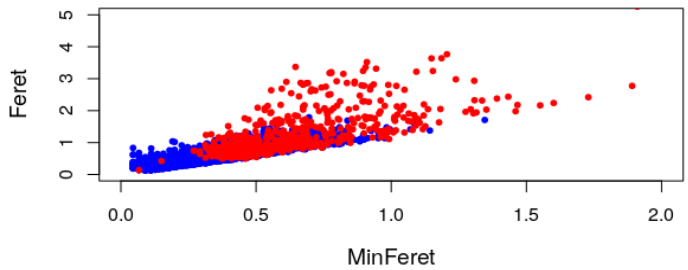

Fig. 13. Particle size distribution in sample 1. *Red* dots are the light particles, *blue* dots are the background

For the remaining samples, the same dependences are also constructed as for sample 1.

Figures 14-20 illustrate the compatible particle size distribution diagrams for the remaining samples.

As demonstrated in Figures 14-20, a more pronounced observation emerges regarding the decline in the number and size of the light particles, concurrently accompanied by an increase in the quantity of the background particles. The parameters of the log-normal distribution of particle sizes, μ and σ, are determined by the following formula:

$$f_x(x) = \frac{1}{\sigma x\sqrt{2\pi}} e^{\frac{-(lnx-\mu)^2}{2\sigma^2}}$$

The distribution mode and median values can provide direct insight into the typical particle sizes in each sample. The mode represents the most frequent particle size, while the median indicates the value at which 50% of particles have a size greater than and 50% smaller than. We don't use an arithmetic mean because in the presence of a long tail of larger particles, it becomes a poor descriptor of typical particle size. Therefore, median and mode are preferred in nanomaterials and particulate systems for their statistical stability and clearer physical interpretation.

A mode and a median can be directly calculated from the log-normal distribution parameters μ and σ:

$$\text{Median} = e^{\mu}$$

$$\text{Mode} = e^{\mu-\sigma^2}$$

The results of determining the parameters of the log-normal distribution, the number of particles, the mode, and the median values of sizes (widths and lengths) for both the light particles and the background particles are summarised in Tables 3-6.

Regarding the width of the light particles across the samples, μ ranges from –0.503 to –0.821, indicating a general shift toward smaller particle sizes in later samples. Similarly, σ decreases from 0.426 to 0.209, suggesting a narrowing of the size distribution and greater uniformity in particle width. The mode and median values follow this

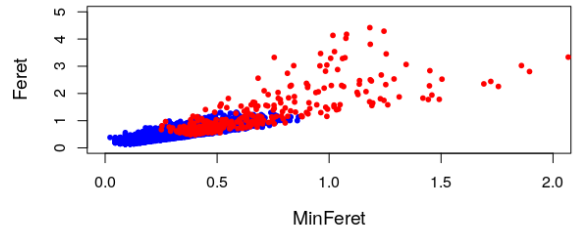

Fig. 14. Particle size distribution for sample 2.

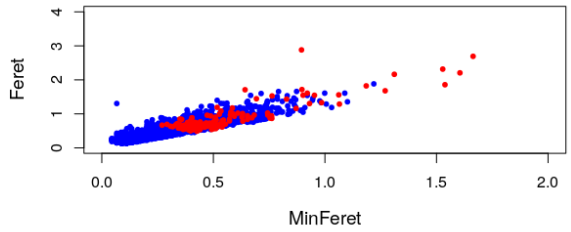

Fig. 15. Particle size distribution for sample 3.

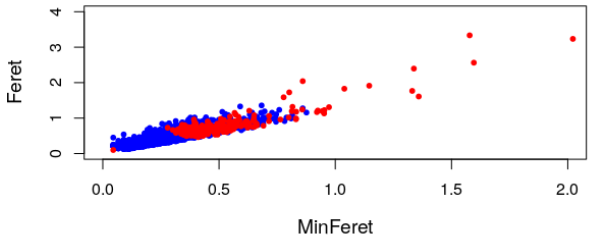

Fig. 16. Particle size distribution for sample 4.

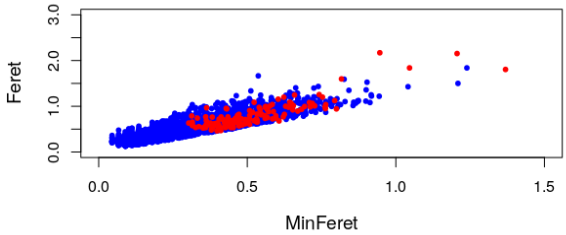

Fig. 17. Particle size distribution for sample 5.

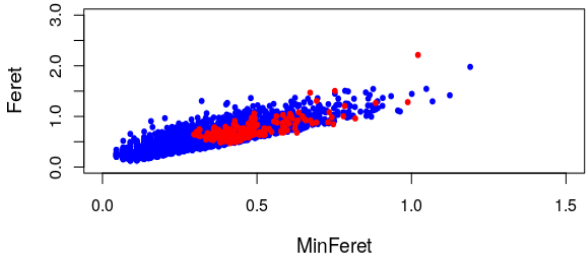

Fig. 18. Particle size distribution for sample 6.

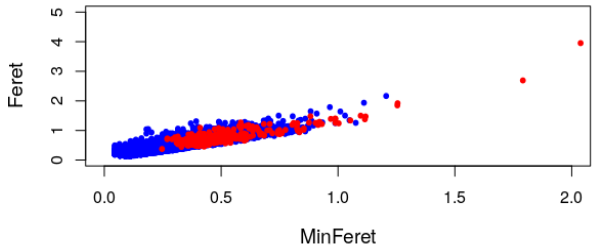

Fig. 19. Particle size distribution for sample 7.

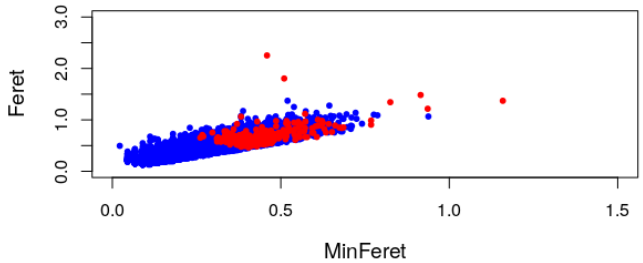

Fig. 20. Particle size distribution for sample 8.

Table 3.

The results of investigation of the width of the light particles

Sample	μ	deviation μ	σ	deviation σ	Number of particles	mode, nm	median, nm
1	-0.503	0.016	0.382	0.012	551	522	605
2	-0.503	0.024	0.426	0.017	326	504	605
3	-0.667	0.029	0.359	0.021	149	451	513
4	-0.732	0.020	0.331	0.014	285	431	481
5	-0.695	0.022	0.269	0.016	144	464	499
6	-0.785	0.015	0.227	0.011	221	433	456
7	-0.750	0.015	0.298	0.010	403	432	472
8	-0.821	0.012	0.209	0.009	280	421	440

Table 4.

The results of investigation of width of the background particles

Sample	μ	deviation μ	σ	deviation σ	Number of particles	mode, nm	median, nm
1	-1.348	0.008	0.544	0.006	4772	193	260
2	-1.363	0.006	0.477	0.004	7145	204	256
3	-1.415	0.009	0.539	0.006	3865	182	243
4	-1.459	0.008	0.479	0.005	3989	185	233
5	-1.353	0.008	0.519	0.005	4523	197	258
6	-1.315	0.008	0.535	0.006	4119	202	268
7	-1.462	0.005	0.521	0.004	10753	177	232
8	-1.484	0.004	0.464	0.003	12523	183	227

Table 5.

The results of investigation of the length of the light particles

Sample	μ	deviation μ	σ	deviation σ	Number of particles	mode, nm	median, nm
1	0.134	0.021	0.492	0.015	551	897	1143
2	0.056	0.030	0.542	0.021	326	788	1057
3	-0.235	0.031	0.373	0.022	149	688	791
4	-0.322	0.019	0.326	0.014	285	652	725
5	-0.279	0.024	0.293	0.017	144	694	756
6	-0.363	0.015	0.229	0.011	221	660	695
7	-0.323	0.014	0.279	0.010	403	670	724
8	-0.398	0.013	0.215	0.009	280	641	672

Table 6.

The results of investigation of the length of the background particles

Sample	μ	deviation μ	σ	deviation σ	Number of particles	Mode nm	median, nm
1	-0.810	0.007	0.482	0.005	4772	353	445
2	-0.862	0.005	0.420	0.004	7145	354	422
3	-0.901	0.008	0.489	0.006	3865	320	406
4	-0.974	0.007	0.436	0.005	3989	312	378
5	0.827	0.007	0.454	0.005	4523	356	437
6	-0.768	0.007	0.458	0.005	4119	376	464
7	-0.922	0.004	0.451	0.003	10753	325	398

trend, decreasing consistently across the series, confirming the presence of finer and more monodisperse particles in samples 6–8. Overall, the results suggest a progression toward smaller, more size-homogeneous particles across the sample set.

The standard deviations of μ are relatively low (0.012–0.029), suggesting that the estimates of the logarithmic mean are statistically reliable. Similarly, the values of σ, which describe the spread of the log-transformed particle size distribution, decrease from 0.426 to 0.209, reflecting a reduction in polydispersity. The deviations of σ are also minor (0.009–0.021), indicating good precision in estimating distribution width.

The mode and the median decrease progressively – the mode drops from 522 nm to 421 nm, and the median from 605 nm to 440 nm – indicating a consistent reduction in particle size. The slight difference between the mode and median in each sample suggests moderate skewness, typical of lognormal distributions. As the particle size becomes smaller, the mode and median also converge

Table 7.

Comparison of minimum and maximum sizes of the light particles

Sample	Width, micron			Length, micron			min/min	max/max
	min	max	max/min	min	max	max/min		
1	0,067	2,29	34,2	0,137	5,26	38,4	2,05	2,29
2	0,251	2,068	8,24	0,486	4,42	9,0973	1,94	2,14
3	0,270	1,664	6,16	0,491	2,88	5,87	1,82	1,73
4	0,045	2,022	44,9	0,100	3,33	33,3	2,22	1,65
5	0,303	1,369	4,52	0,463	2,17	4,69	1,53	1,59
6	0,296	1,021	3,45	0,472	2,21	4,69	1,60	2,17
7	0,247	2,038	8,25	0,374	3,95	10,6	1,51	1,94
8	0,261	1,159	4,44	0,463	2,25	4,87	1,77	1,94

Table 8.

Comparison of minimum and maximum sizes of the background particles

Sample	Width, micron			Length, micron			min/min	max/max
	min	max	max/min	min	max	max/min		
1	0,045	1,346	29,9	0,127	1,79	14,1	2,82	1,33
2	0,022	0,863	39,2	0,131	1,31	10,0	5,96	1,52
3	0,045	1,219	27,9	0,127	1,88	14,8	2,82	1,54
4	0,045	0,876	19,5	0,127	1,36	10,7	2,82	1,55
5	0,045	1,239	27,5	0,127	1,84	14,5	2,82	1,48
6	0,045	1,190	26,4	0,127	1,98	15,6	2,82	1,66
7	0,045	1,206	26,8	0,131	2,17	16,5	2,91	1,80
8	0,022	0,938	42,6	0,127	1,37	10,8	5,77	1,46

slightly, which may reflect a more symmetric and narrow distribution in later samples. These trends confirm the tendency toward finer and more uniform particles in the investigated series.

In the table is summarised the result of approximation sampling distribution of the partical width by lognormal one. A decrease in μ implies that the median particle diameter (D_{50}) has shifted to a smaller value. Calculation of change in median diameter:

$$D_{50}=e^{\mu}$$

When $\mu = -0.503 \rightarrow D_{50}=e^{-0.503}\approx 0.605$
When $\mu = -0.821 \rightarrow D_{50}=e^{-0.821}\approx 0.440$

So the median diameter decreased by ~27%, meaning particles are, on average, getting smaller.

The geometric standard deviation (GSD) – which reflects how spread out the particle sizes are – is:

$$GSD=e^{\sigma}$$

For $\sigma = 0.382 \rightarrow GSD \approx e^{0.382}\approx 1.465$
For $\sigma = 0.209 \rightarrow GSD \approx e^{0.209}\approx 1.232$

This shows a decrease in spread: particles are now more uniform in size.

As illustrated in Table 3, the mode undergoes a transition from 0.522 to 0.421 μm, and the mean width value declines from 0.65 to 0.45 μm. The number of particles also exhibits a decrease, though this change is less pronounced, in response to an increase in the initial concentration of TU in the electrolyte.

The data in Tables 4 and 5 show that the sizes of the background particles are significantly smaller in width (about twice as large) than those of the light particles. The mode and mean sizes of the background particles are only slightly dependent on the concentration of TU. The number of background particles is several tens higher than the number of light particles.

The tabular data presented for particle length show a similar trend to the data for width: light particles slightly decrease their average size with increasing TU concentration, while background particles change little in both mode and mean. Similarly, the average length of background particles is 2.5÷1.5 times smaller than that of the light particles.

The minimum and maximum particle sizes in width

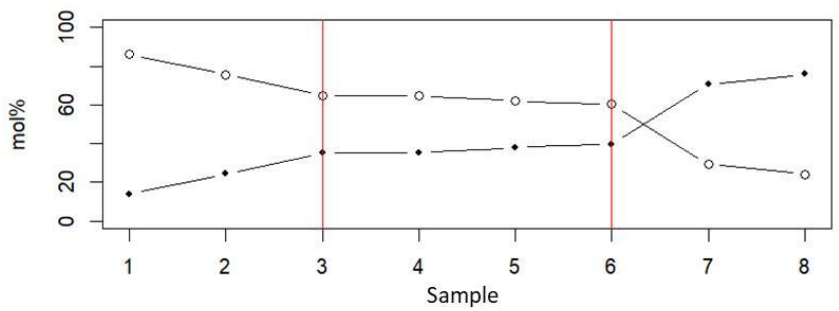

Fig. 21. The content of ZnO/ZnS of the samples.

and length and the ratio of minimum and maximum sizes are also determined. These data are given in Tables 7 and 8.

These data suggest that the background particles are smaller than the light particles (approximately in 2 times). However, there is significant scatter in particle size and a lognormal distribution for all particles shown. Also, we observed the following issue (Figure 21) in the experiment:

There are therefore two important points to note: in the first case, large crystals disappear, and in the second, at lower concentrations of TU, there is a high probability that zinc sulfide will not have time to form, and zinc oxide will predomi nate in the mixture. There is therefore a limiting concentration of TU above which zinc sulfide is the predominant product.

Conclusions

As shown by the results of electron microscopy and energy dispersive analysis, electrolysis of an aqueous solution of sodium chloride and TU with a soluble anode at constant temperature and constant current density allows obtaining ZnO and ZnS composites. Increasing the TU content in the electrolyte changes the composition of the composite powders from a higher content of the light particles to a higher content of background particles in the mixture and reduces the size of the light particles in length by a factor of 2 and in width by a factor of 1.5. The concentration of TU has no significant effect on the size of the background particles. However, the content of ZnS increases with thiourea concentration because TU provides the sulfur source necessary for ZnS formation, and its higher availability enhances both sulfidation and precipitation reactions involving zinc species. The background particles are smaller than the light particles.

Notes

The authors declare no competing financial interest.

Yanchuk O.M. *– Candidate of Chemical Sciences, Associate Professor of Volyn Medical Institute;*
Smitiukh O.V. *– Candidate of Chemical Sciences, Associate Professor of the Department of Inorganic and Physical Chemistry; Lesya Ukrainka Volyn National University;*
Marchuk O.V. *– Doctor of Chemical Sciences, Professor of the Department of Inorganic and Physical Chemistry, Lesya Ukrainka Volyn National University;*
Suprunovich S.V. *– Candidate of Chemical Sciences, Associate Professor of the Department of Organic Chemistry and Pharmacy, Lesya Ukrainka Volyn National University;*
Kordan V.M. *– Candidate of Chemical Sciences, Senior Researcher at the Department of Inorganic Chemistry, Ivan Franko National University of Lviv.*

[1] K. Ravichandran, P.K. Praseetha, T. Arun, S. Gobalakrishnan, *Synthesis of Nanocomposites*. Synthesis of Inorganic Nanomaterials, 141 (2017); https://doi.org/10.1016/B978-0-08-101975-7.00006-3.
[2] Parita Basnet, Dhrubajyoti Samanta, Somenath Chatterjee. *Chemical Approach Based ZnS-ZnO Nanocomposite Synthesis and Assessment of their Structural, Morphological and Photocatalytic Properties*. Journal of Nano- and Electronic Physics, 13(1), 01025 (2021); https://doi.org/10.21272/jnep.13(1).01025.
[3] M. Sundararajan, P. Sakthivel, A.C. Fernandez, *Structural, optical and electrical properties of ZnO-ZnS nanocomposites prepared by simple hydrothermal method*. Journal of Alloys and Compounds, 768, 553 (2018); https://doi.org/10.1016/j.jallcom.2018.07.245.
[4] K. Benyahia, F. Djeffal, H. Ferhati, A. Benhaya, A. Bendjerad, Y. Djaballah, N. Martin, *Microstructured ZnO-ZnS composite for earth-abundant photovoltaics: Elaboration, surface analysis and enhanced optical performances.* Solar Energy, 218, 312 (2021); https://doi.org/10.1016/j.solener.2021.02.057.
[5] Y. Tsai, T. Chou, C. Y. Xu, W. Chang Huang, C.F. Lin, Y.S. Wu, Y. Lin, H. Chen, *ZnO/ZnS core-shell nanostructures for hydrogen gas sensing performances.* Ceramics International, 45(14), 17751 (2019); https://doi.org/10.1016/j.ceramint.2019.05.345.
[6] O.V. Smitiukh, O.V. Marchuk, O.M. Yanchuk, Yu.O. Khmaruk, D.S. Zhernov, *Nanoparticles of ZnO/ZnS: Electrochemical Synthesis, Analysis and Prospective Applications.* Journal of Nano- and Electronic Physics, 16(1), 01024 (2024); https://doi.org/10.21272/jnep.16(1).01024.
[7] H.M. Talib, A.A.Yousif, A.H. Omran Alkhayatt, *The impact of TU concentration on the Structural, surface morphologyand optical characterization of chemically deposited CdS-PVA nanocomposites thin films*. Results in Optics, 15, 100641 (2024); https://doi.org/10.1016/j.rio.2024.100641.
[8] P. Scherrer, *Nachrichten von der Gesellschaft der Wissenschaften zu Göttingen*, Mathematisch-Physikalische Klasse, 2, 98 (1918);
[9] C.A. Schneider, W.S. Rasband, K.W. Eliceiri, NIH Image to ImageJ: 25 years of image analysis, *Nat Methods.* 9 (7), 671 (2012); https://doi.org/10.1038/nmeth.2089.

О.М. Янчук[1], О.В. Смітюх[2], О.В. Марчук[2], С.В. Супрунович[2], В.М. Кордан[3]

Вплив концентрації тіосечовини на хімічний склад, морфологію та розподіл частинок нанокомпозиту ZnO/ZnS, отриманого методом електрохімічного анодування

[1]*Волинський медичний інститут, Луцьк, Україна, yanchuk59@gmail.com*
[2]*Волинський національний університет імені Лесі Українки, Луцьк, Україна, Smitiukh.Oleksandr@vnu.edu.ua*
[3]*Львівський національний університет імені Івана Франка, Львів, Україна, vasyl.kordan@lnu.edu.ua*

У представленому дослідженні вивчено вплив різних концентрацій тіосечовини (TU) на синтез і властивості нанокомпозитів ZnO/ZnS, отриманих методом електрохімічного анодування. Тіосечовина виступала джерелом сірки, що забезпечувало формування ZnS у матриці ZnO. Структурні, морфологічні та композиційні дослідження виконано з використанням методу рентгенівської дифракції (XRD), скануючої електронної мікроскопії (Tescan Vega3 LMU), програмного забезпечення ImageJ з плагінами ParticleSizer (для великих кристалів) і MorphoLibJ (для фону), а також енергодисперсійної рентгенівської спектроскопії (EDX).

Аналіз хімічного складу підтвердив, що зі зростанням концентрації тіосечовини збільшується вміст ZnS. Підвищення концентрації TU в електроліті змінює склад композитних порошків, зсуваючи баланс від переважання світліших частинок до більшої частки фонових частинок у суміші. Це також призводить до суттєвого зменшення розмірів світліших частинок: їх довжина зменшується вдвічі, а ширина – у 1,5 раза. Крім того, такі зміни складу та розмірів частинок можуть впливати на загальні властивості та експлуатаційні характеристики композитних матеріалів.

Параметри μ та σ зменшуються зі збільшенням концентрації тіосечовини, що свідчить про зменшення середнього розміру частинок і підвищення їх однорідності. Значення моди та медіани демонструють аналогічну тенденцію, послідовно зменшуючись у межах серії, що підтверджує наявність дрібніших і більш монодисперсних частинок у зразках 6–8. Розуміння цих взаємозв'язків є важливим для оптимізації складу матеріалів відповідно до конкретних вимог у таких галузях, як електроніка, зберігання енергії та сучасне виробництво.

Ключові слова: тіосечовина, нанокомпозити, анодування, морфологія.